First Benchmark of Relativistic Photoionization Theories against 3D ab initio Simulation

B. Hafizi, D. F. Gordon, and J. P. Palastro

Phys. Rev. Lett. **118**, 133201 — Published 28 March 2017

DOI: 10.1103/PhysRevLett.118.133201

First benchmark of relativistic photoionization theories against 3D *ab initio* simulation

B. Hafizi, D.F. Gordon and J.P. Palastro

Naval Research Laboratory, Washington DC 20375

Abstract

Photoelectron spectra and ionization rates encompassing relativistic intensities and hydrogen-like ions with relativistic binding energies are obtained using a quasi-classical *S*-matrix approach. These results, along with those based on the imaginary time method, are compared with 3D, ½-period *ab initio* simulations for a wide range of ionization potentials and electric field amplitudes. Significant differences between the three results are demonstrated. Time-dependent simulations indicate that the peak ionization current can occur before the peak of the electric field.

Advances in laser technology are expanding the frontiers of high-field science. An extreme example is vacuum polarization, in which an intense laser near the Schwinger field creates electron-positron pairs. In the near term, one has photoionization of increasingly relativistic bound states, and an urgent need to understand the limitations of current models. Horizon laser systems, such as the Extreme Light Infrastructure, will be able to fully strip heavy elements via tunneling ionization. Ultimately, both the quantum mechanical bound electron dynamics and free electron motion must be treated relativistically.

Relativistic photoionization implies a binding energy comparable to the electron rest mass or a light intensity sufficient for relativistic photoelectron dynamics. When both are true, the abundance of photons permits a semi-classical treatment of the light field. The relativistic binding energies and resulting photoelectron kinetic energies, however, require a covariant quantum description of the electronic wavefunction, i.e. the Dirac or Klein-Gordon (K-G) equations. There are two analytical approaches for determining the photoelectron spectra and ionization probabilities [1-4]. The imaginary time method (ITM) employs a Feynman propagator to evolve the electronic wavefunction from its initial bound state to a final state [3]. The ionization probability is found by minimizing an action functional along electron trajectories integrated in imaginary time through the classically forbidden region. In the second approach, an S-matrix is defined as an overlap integral between a bound state in the distant past and a free, final state in the remote future [1].

The two approaches involve several approximations and until now their predictions have never been tested against fully relativistic 3D *ab initio* simulations. Even in 2D only a few nascent explorations appear in the literature [5-7]. The purpose of this paper is to obtain the ionization rate of hydrogen-like ions in the regime of relativistic binding (i.e., high charge states) and relativistic photoelectron dynamics (i.e., high laser intensities) and compare the results with 3D, ½-period *ab initio* simulations.

The ionization rates for the K-G and Dirac equations were calculated using the imaginary time method in [8,9]. Here, using the *S*-matrix approach, a novel ionization rate is derived for the K-G equation. The procedure resembles the one used in [10] for the Dirac equation. For all cases considered here, the applied radiation field is taken as a plane wave.

To parallel the Dirac equation analysis, the two-component form of the K-G equation $i\hbar\partial_t\Psi=\hat{H}\Psi$ is employed [11]. Here $\hat{H}=(\hat{\mathbf{P}}-e\mathbf{A}/c)^2(\hat{\tau}_3+i\hat{\tau}_2)/2m+e\phi+mc^2\hat{\tau}_3+eV$ is the Hamiltonian operator, $\hat{\mathbf{P}}$ is the momentum operator, e and m are the electronic charge and mass, respectively, c is the speed of light *in vacuo*, $V(\mathbf{r})$ is the Coulombic potential due to the nucleus, $(\phi,\mathbf{A})$ are the electromagnetic scalar and vector potentials, $(\hat{\tau}_1,\hat{\tau}_2,\hat{\tau}_3)$ are the Pauli matrices and $\Psi=\begin{pmatrix}\varphi(\mathbf{r},t)\\ \chi(\mathbf{r},t)\end{pmatrix}$ is a two-component state vector defined in terms of the solution ψ of the second-order K-G equation by $\varphi\equiv\frac{1}{2}(\psi+i\hbar\psi^0/mc^2)$, $\chi\equiv\frac{1}{2}(\psi-i\hbar\psi^0/mc^2)$ and $\psi^0\equiv[\partial_t+ie(\phi+V)/\hbar]\psi$. The charge density is given by $\rho(\mathbf{r},t)=e[|\varphi(\mathbf{r},t)|^2-|\chi(\mathbf{r},t)|^2]=e\Psi^\dagger(\mathbf{r},t)\hat{\tau}_3\Psi(\mathbf{r},t)$, where $\Psi^\dagger(\mathbf{r},t)=(\varphi^*,\chi^*)$ denotes the adjoint vector. Note that the two components of Ψ represent the charge—and not the spin—of the particle [11].

The *S*-matrix $(S-1)_{fi}=-(i/\hbar)\int_{-\infty}^{\infty}dt(\hat{H}_1\Psi_f,\Phi_i)$ expresses the transition probability between the initial Φ_i and the final Ψ_f state vectors, where $\hat{H}_1$ is the part of the total Hamiltonian dependent on the laser field (*Supplemental Material* [12]). For hydrogen-like ions a Coulombic potential $V(r)=-Ze/r$ with atomic number Z binds the electron to the nucleus. If the electron starts in the ground state (1*s*), the initial state vector is

$$\Phi_i(\mathbf{r},t)=\frac{1}{2}\begin{pmatrix}1+\dfrac{E_0-eV}{mc^2}\\ 1-\dfrac{E_0-eV}{mc^2}\end{pmatrix}e^{-iE_0t/\hbar}\psi_0(\mathbf{r})$$

where $\psi_0(\mathbf{r})=C_{1s}(r/r_0)^{(E_0/mc^2)^2-1}e^{-r/r_0}/\sqrt{\pi r_0^3}$ is the eigenfunction with energy eigenvalue $E_0/mc^2=\sqrt{\frac{1}{2}+\sqrt{\frac{1}{4}-(Z\alpha)^2}}$, $\alpha=e^2/\hbar c$, $r_0=\lambda\!\!\!^{-}_C/\sqrt{1-(E_0/mc^2)^2}$ is the ground state radius and $\lambda\!\!\!^{-}_C=\hbar/mc$ is the reduced Compton wavelength. Employing the normalization $\int d^3r\,\rho(\mathbf{r})=e$ leads to $C_{1s}^2=2^{2(E_0/mc^2)^2-1}(E_0/mc^2)/\Gamma[2(E_0/mc^2)^2+1]$ where $\Gamma(x)$ is the gamma-function. The

ionization energy I_p is defined by $E_0/mc^2 \equiv 1 - I_p/mc^2$. Note that E_0 becomes imaginary when $Z\alpha > 1/2$, providing the maximum atomic number $Z = 68$ for a K-G 'atom'.

To lowest order, Ψ_f is proportional to the Volkov wavefunction, $\Psi_f \propto e^{i S_{em}/\hbar}$, where S_{em} is the classical action of an electron in a plane electromagnetic wave [17,18]. The correction $S_{em} \rightarrow S_{em} + S_{Coulomb}$ due to the Coulomb potential of the nucleus can be computed as in [10]. The electric field gauge is used to express the vector potential as $A^\mu = [-y E_y \cos(\omega\xi/c), -y E_y \cos(\omega\xi/c), 0, 0]$, where E_y is the electric field amplitude, $\omega = 2\pi c/\lambda$ is the frequency, λ is the wavelength and $\xi = ct - x$. The electric field gauge, which emphasizes large distances from the nucleus, is well-suited to the quasi-classical approximation of the wavefunction [10, 19].

The *S*-matrix total ionization rate averaged over a wave period is given by (*Supplemental Material* [12])

$$\langle w \rangle \approx \frac{c}{\mathrm{D}_C} \frac{2^{(\nu-1)/2 - 40 I_p/9mc^2} [\Gamma(\frac{\nu}{2})\, C_{1s}]^2}{3^{3/4}\sqrt{\pi}\ \alpha^{3(\nu - 3/2 - 20 I_p/9mc^2)}} \left(\frac{mc^2}{E_0}\right)^{2\nu} \left(\frac{\mathrm{D}_C}{r_0}\right)^{2(2\nu - 3/2 - 10 I_p/9mc^2)} \left(\frac{I_p}{mc^2}\right)^{(3-\nu)/2 - 20 I_p/9mc^2}$$

$$\times \frac{G(1+\Xi^2)}{\Xi^{5/2}\sqrt{1+\Xi^2/3}} \frac{[1 - I_p/3mc^2 + (I_p/mc^2)^2/27]^{\nu - 1 + 20 I_p/9mc^2}}{(E_y/E_a)^{\nu - 3/2 - 20 I_p/9mc^2}} e^{(29/9) Z\alpha \sqrt{I_p/2mc^2}}\ e^{-2E_c/3E_y} \quad ,$$

$$\times \left(\left\{ 1 + \frac{E_0}{mc^2}\left[1 + \frac{I_p}{3mc^2} + \frac{2}{27}\left(\frac{I_p}{mc^2}\right)^2 \right] \right\}^2 + 2^{3/2}\alpha^3 \left[\frac{\Gamma(\frac{1+\nu}{2})}{\Gamma(\frac{\nu}{2})}\right]^2 \frac{E_y}{E_a}\sqrt{\frac{I_p}{mc^2}}\left[1 - \frac{I_p}{3mc^2} + \frac{1}{27}\left(\frac{I_p}{mc^2}\right)^2 \right] \right)$$

(1)

where $E_a \equiv \alpha^3 E_S$, $E_S = m^2c^3/|e|\hbar$ is the Schwinger field, $E_c \equiv (\sqrt{3}\,\Xi)^3 (1+\Xi^2)^{-1} E_S$ defines a characteristic electric field that is nearly equal to the field on the *K*-shell of a hydrogen-like atom, $E_0/mc^2 = (1-\Xi^2)/\sqrt{1+\Xi^2}$ defines Ξ, $\nu \approx 2 - E_0/mc^2 + (E_0/mc^2)^2$, $G \approx 1 - (13/8 + q)[3E_y/2E_c] + \frac{1}{2}(1257/64 + 45q/4 + 3q^2)[3E_y/2E_c]^2$ and $q = 10 I_p/9mc^2 - (1+\nu)/2$.

The analysis leading to Eq. (1) makes use of the quasi-static (tunneling), the quasi-classical and the saddle point approximations. These are valid when the barrier width normalized by the atomic radius is large, $\sqrt{2}\,(I_p/mc^2)^{3/2} E_S/E_y \gg 1$, the relativistic Keldysh

parameter is small, $\gamma_R \equiv mc\omega\sqrt{3\Xi^2/(1+\Xi^2)}/|eE_y| = 1$, and the electromagnetic frequency normalized by the atomic frequency is small, $\hbar\omega/I_p = 1$. In what follows, parameters are chosen so that these requirements are satisfied (*Supplemental Material* [12]). Wavemechanical interference is omitted in Eq. (1). These same approximations apply to the rate based on the imaginary time method. It should be pointed out that the approximation $I_p/mc^2 = 1$ is made at various stages in obtaining Eq. (1)—specially in connection with evaluating the Coulomb effect of the nucleus. Whilst the validity of ITM is claimed to extend to $I_p/mc^2 = 1$ [8], the analytical form for the Coulomb correction is only derived for constant, uniform, crossed electric and magnetic fields [20].

Ab initio simulations are not limited by any of the above restrictions. Three-dimensional numerical solutions of the K-G equation were obtained using the model described in [5]. Controls on numerical errors and validation are discussed there. The calculations here are limited to ½-period of the radiation field to reduce computational expense. Even then, 3D simulations require 2^{16} central processing unit cores, with $2^{13}\times 2^{13}\times 2^{10}$ cells and 2^{16} steps. The ionization rate is computed by integrating the charge outside a suitable sphere surrounding the core, after one half-period of the radiation, and dividing by $e\lambda/2c$. The wavelength of the radiation is chosen so that the numerical accuracy and computation time are fixed for any chosen ionization potential. The peak electric field is fixed according to the barrier suppression ionization threshold (BSI) [21]. The BSI formula depends on the nuclear charge. The soft core potential of the numerical atom is chosen to give the Dirac ground state energy associated with this charge. It turns out that the BSI electric field leads to a barrier width [9] that is sufficiently large for the quasiclassical approximation to be applicable (Fig. 1, *Supplemental Material* [12]). Simulations in 2D—where motion along the magnetic field (z-axis) is completely neglected—have also been performed. Simulations in 2D serve several purposes. First, it is of interest to understand the effect of dimensionality on ionization rates. Second, numerical convergence studies in 2D can be used to determine acceptable resolution in 3D. Finally, simulations in 2D can be run over longer time scales. Convergence was also directly verified in 3D by varying the cell size along the z-axis (*Supplemental Material* [12]).

The characteristic field $E_c(I_p)$ is determined once the ground state energy is chosen. For the ionization energies considered herein $I_p/mc^2 = 0.00866, 0.0351, 0.0809, 0.158, 0.259$, the corresponding normalized (peak) electric fields are $E_y/E_c(I_p) = -0.0630, -0.0635, -0.0643, -0.0662, -0.0684$, respectively. Note that the normalized electric field is nearly constant across the range of ionization energies.

Figures 1 (a) and (b) are snapshots of charge density for $I_p/mc^2 = 0.259$ and peak electric field $E_y/E_c = -0.0684$ early-on in the interaction ($ct/\lambda = 1/4$) and after ($ct/\lambda = 3/8$) a piece has detached from the core, respectively. Notable features include the manner in which the charge density bends in the direction of the radiation momentum, and the spread in the direction of the magnetic field. These highlight the 3D nature of the wavefunction.

Figure 2 provides the first comparison of the analytically-closed form ionization rates (averaged over an optical period) with fully relativistic, 3D *ab initio* simulations. In particular, the figure shows a comparison of the ionization rate obtained from *S*-matrix calculations [Eq. (1), above], ITM calculations [Eq. (4.2) in Ref. 8] with those from simulations. The lower abscissa in Fig. 2 is the ionization potential I_p/mc^2 whilst the upper abscissa gives the values for the normalized vector potential $a = |e|E_y/mc\omega$. The ITM and *S*-matrix rates shown in Fig. 2 differ even when $I_p/mc^2 = 1$ because multiphoton ionization is included in the former but not in the latter (in the extreme tunneling limit $\gamma_R \to 0$ the two rates are the same; see *Supplemental Material* [12]). Note that the ITM rate tracks the simulated rate more closely in the relativistic limit. For comparison simulation results in 2D are also shown. Additionally the prediction of the time-dependent Schrödinger equation (TDSE) is given, in the case $I_p/mc^2 = 9.60\times10^{-4}$ where the parameters are non-relativistic, using the algorithm of [22]. The result coincides with the 3D K-G simulation as expected. The dipole approximation, a sometime point of contention [1], is used in the TDSE simulation, but not in any of the K-G simulations.

Fig. 2 shows that both theoretical treatments overestimate the 3D ionization rate, while coming close to the 2D ionization rate. The analytical calculations can in principle be performed in three dimensions; in practice, however, the $z-$dimension is treated as an ignorable coordinate.

For example, in the calculation of the Coulomb factor, only trajectories with $z = 0$ are considered. This is a likely contributor to the behavior in Fig. 2. In this connection it should also be recalled that in the analytical approaches the electron path associated with the lowest-order action S_{em} is a figure-8 confined to the $x, y-$plane. The central potential associated with the Coulomb potential of the nucleus, however, which breaks this symmetry, is only computed as a perturbation.

In order to verify that the simulated ionization rate is computed accurately, it was confirmed that the flow of current through the diagnostic surface is insignificant at the time the ionized charge is evaluated. The radius of the diagnostic sphere in all cases was 20 ground state radii (see Ref. 23 for a discussion of dependence on radius of diagnostic sphere).

Simulations make use of the vector potential such that the peak of the electric field occurs at $\varphi = 0$, where $\varphi \equiv -\pi/2 + \omega\,\xi/c = -\pi/2 + \omega\,(ct - x)/c$ is the phase (*Supplemental Material* [12]). Whilst resolution, accuracy and convergence have been ensured, it has been necessary to constrain the duration of the laser pulse in 3D simulations to just half-a-period. Although such a field is physically realizable the derivative of the electric field is non-vanishing at the onset of the pulse and it should be remembered that the theory applies to a slowly-varying envelope--even though, according to theory, the ionization rate is determined by the conditions at a single phase of the radiation field. Because the whole space-time dependence of the wavefunction falls out of the *ab initio* simulations it is possible to examine the ionization rate $w(t)$ as a dynamical quantity and to identify its dependence on the pulse shape. In particular, the current flowing through a sufficiently large sphere surrounding the ion is equated with the instantaneous ionization rate. Figure 3 displays the instantaneous ionization rate as a function of φ for $I_p / mc^2 = 0.259$. The solid curve in Fig. 3 is for a 3D, ½-period pulse and the long-dash curve is the corresponding 2D result. An important and counter-intuitive feature of both is that the phase at which the peak photoelectron current is obtained is earlier in time than the peak of the electric field. This is not a result of ground state depletion, which in all cases treated here is insignificant, and implies that for certain parameters, increasing the field strength reduces the ionization rate. This time-dependent phenomenon is to be compared with the well-known stabilization phenomenon in which an applied field creates a bound state that is more stable against ionization than the usual

one [1, 24-26]. In the latter the bound state develops over many radiation periods. The complex behavior for a ½-period pulse is not captured by any of the analytical rates. To see how the onset of the pulse affects this behavior, the dotted curve in Fig. 3 shows the results of a 2D simulation in which the pulse builds up over 3 optical periods. Now it is seen that the time at which the peak of the photoelectron current occurs is later than that of the electric field.

The first comparison of 3D, ½-period relativistic *ab initio* simulations with analytical *S*-matrix and imaginary time method (ITM) tunneling ionization rates reveals the following. The analytical ionization rates overestimate the ionization rate derived from simulations by nearly an order of magnitude in the relativistic limit, with the ITM rate tracking the simulated rate more closely. It is also found that 2D simulations overestimate the ionization rate in a similar way, suggesting that the limitations of the analyses stem, in part, from neglecting the coordinate dimension parallel to the magnetic field. The simulation results contain temporal information on the ionization rate that is not captured by the saddle point approximation used in the analytical methods. In particular, ½-period pulses are found to give unique ionization dynamics. Experimentally, measurement of the momentum distribution can shed light on the ionization dynamics. Experimental tests of tunneling ionization rates for $I_p / mc^2 \approx 1/4$ require fields on the order of 10^{16} V/m.

Acknowledgment

This work was supported by NRL 6.1 Base Funds and by DoE. Large scale computer simulations were carried out using resources provided by the DoE National Energy Research Supercomputing Center and the DoD High Performance Computing Modernization Program.

References

[1] H.R. Reiss, Prog. Quant. Electr. **16**, 1 (1992).

[2] N.B. Delone and V.P. Kraĭnov, Phys. Usp. **41**, 469 (1998).

[3] V.S. Popov, Phys.-Usp. **47**, 855 (2004).

[4] S.V. Popruzhenko, J. Phys. B: At. Mol. Opt. Phys. **47**, 204001 (2014).

[5] D.F. Gordon, B. Hafizi, and M.H. Helle, J. Comp. Phys. **267**, 50 (2014).
[6] M. Almquist, K. Mattsson, T. Edvinsson, J. Comp. Phys. **262**, 86 (2014).
[7] H. Bauke, C. Keitel, Comput. Phys. Commun. **182**, 2454 (2011).
[8] V.S. Popov, B.M. Karnakov, V.D. Mur and S.G. Pozdnyakov, J. Exp. Theor. Phys. **102**, 760 (2006).

[9] B.M. Karnakov, V.D. Mur and V.S. Popov, J. Exp. Theor. Phys. **105**, 292 (2007).

[10] M. Klaiber, E. Yakaboylu, and K. Hatsagortsyan, Phys. Rev. A **87**, 023417 (2013); *ibid*, **87**, 023418 (2013).

[11] G. Baym, *Lectures on Quantum Mechanics* (Benjamin, 1969), chap. 22.

[12] See Supplemental Material, which includes Refs. [13-16].

[13] F.H.M. Faisal, J. Phys. B **40**, F145 (2007).

[14] F.H.M. Faisal, Phys. Rev. A **75**, 063412 (2007).

[15] C.I. Moore, A. Ting, T. Jones, E. Briscoe, B. Hafizi, R.F. Hubbard and P. Sprangle, Phys. Plasmas **8**, 2481 (2001).

[16] B. Hafizi, P. Sprangle, J.R. Peñano and D.F. Gordon, Phys. Rev. E **67**, 056407 (2003).

[17] H.R. Reiss, Phys. Rev. A **42**, 1476 (1990).

[18] L.D. Landau and E.M. Lifshitz, *The Classical Theory of Fields* (Elsevier, 1975) § 47.

[19] G.F. Gribakin and M.Yu. Kuchiev, Phys. Rev. A **55**, 3760 (1997).

[20] V.D. Mur, B.M. Karnakov and V.S. Popov, J. Exp. Theor. Phys. **87**, 433 (1998).

[21] S. Augst, D. Strickland, D.D. Meyerhofer, S.L. Chin and J.H. Eberly, Phys. Rev. Lett. **63**, 2212 (1989).
[22] D.F. Gordon, B. Hafizi, and A.S. Landsman, J. Comp. Phys. **280**, 457 (2015).
[23] D.F. Gordon and B. Hafizi, J. Comp. Phys. **231**, 6349 (2012)
[24] J.H. Eberly and K.C. Kulander, Science **262**, 1229 (1993).
[25] E.A. Volkova, V.V. Gridchin, A.M. Popov and O.V. Tikhonova, J. Exp. Theor. Phys. **99**, 320 (2004).
[26] F. Morales, M. Richter, S. Patchkovskiĭ and O. Smirnova, Proc. Natl. Acad. Sci. **108**, 16906 (2011).

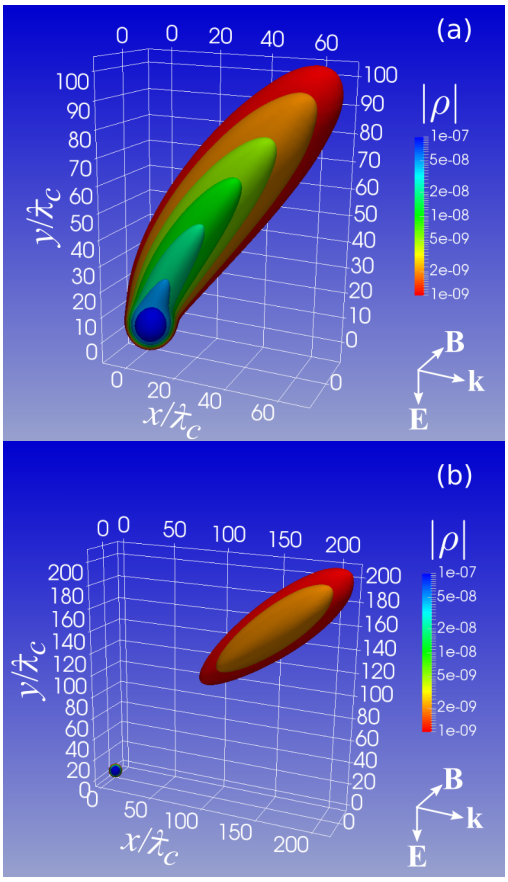

Figure 1. Snapshots of charge density $|\rho| = |e\Psi^{\dagger}(\mathbf{r},t)\hat{\tau}_3\Psi(\mathbf{r},t)|$ at (a) $ct/\lambda = 1/4$ and (b) $ct/\lambda = 3/8$, respectively, obtained from simulations. Ionization potential $I_p/mc^2 = 0.259$ and peak laser electric field normalized to the characteristic electric field $E_y/E_c = -0.0684$. Panel (a) is at the peak of the electric field while for panel (b) the field is reduced by the factor $\sqrt{2}$.

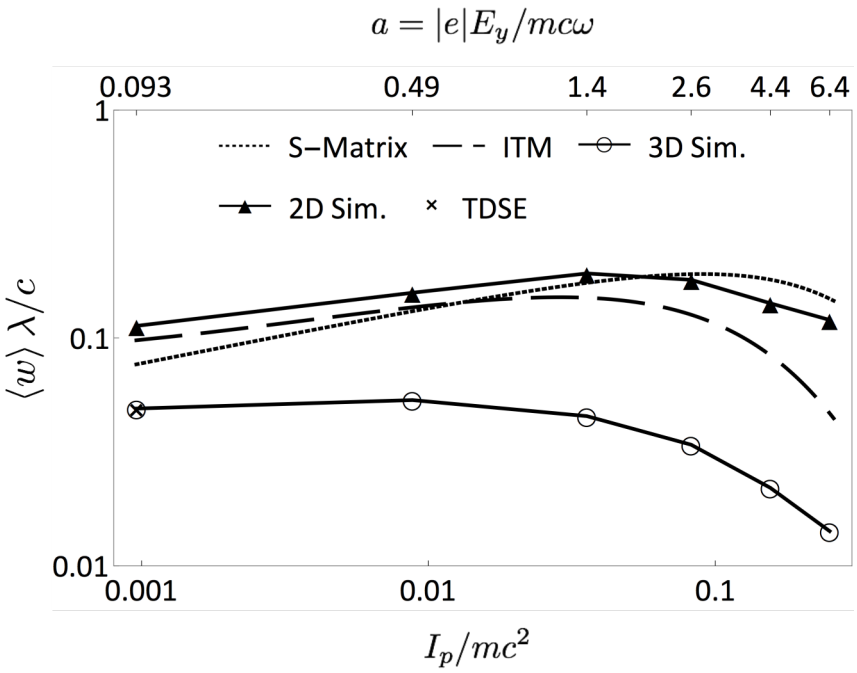

Figure 2. Comparison of ionization rates (averaged over an optical period, normalized by c/λ) based on the $S-$matrix method (dotted), imaginary time method (ITM, dashed), 2-D simulations (triangles) and 3-D simulations (circles) of K-G equation. The "x" marks the result of a high resolution, axisymmetric, time dependent Schrödinger equation simulation (TDSE), in the dipole approximation. The lower and upper abscissæ show the ionization potential and the normalized vector potential, respectively. [Abscissa values yield the relativistic Keldysh parameter $\gamma_R = \sqrt{3\Xi^2/(1+\Xi^2)}/a$, where Ξ is a function of I_p/mc^2 and is defined following Eq. (1)]. The peak laser electric field, normalized to the characteristic electric field, is nearly constant across the plot and listed in the text prior to description of Fig. 1.

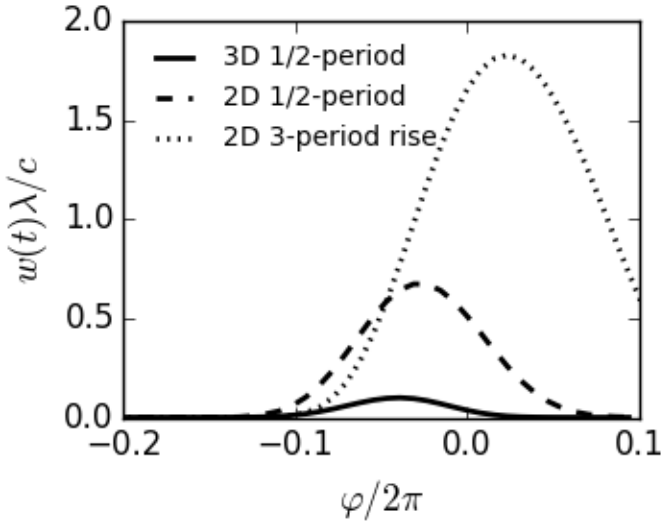

Figure 3. Instantaneous ionization rate (normalized by c/λ) versus the phase of laser pulse for ionization potential $I_p/mc^2 = 0.259$ and peak laser electric field normalized to characteristic electric field $E_y/E_c = -0.0684$. With the half-cycle pulse format, in either 2D or 3D, the peak photoelectron current occurs before the peak of the electric field (at $\varphi \equiv 0$). A case with finite pulse envelope is shown for comparison. Positive phases can be explained as a delay due to finite radius of the diagnostic sphere, but negative phases must be interpreted as a decrease in ionization current with an increase in the field. The ionization fraction (integrated curve) is too small for depletion of the bound state wavefunction to play a role.